EVOLUTION OF RESIDUAL STRESS AND ITS RELATION TO MICROSTRUCTURE IN MULTI-CRYSTALLINE SILICON THIN FILM SOLAR CELLS ON GLASS PREPARED BY COMBINED LASER CRYSTALLIZATION AND SOLID PHASE EPITAXY

G. Sarau[1*], M. Becker[1,2], A. Bochmann[1], A.Gawlik[1], G. Andrä[1], S. Christiansen[1,2]
[1]Institute of Photonic Technology, Albert-Einstein Str. 9, D-07745 Jena, Germany
[2]Max-Planck-Institute of Microstructure Physics, Weinberg 2, D-06120 Halle, Germany
[*]Correspondence: Tel: +49 3641 206401, Fax: +49 3641 206499, E-mail: george.sarau@ipht-jena.de

ABSTRACT: Stress engineering in thin film solar cells on foreign substrates represents an important manufacturing issue to prevent cracking or peeling off the film or even substrate warpage resulting in an increased breakage risk and processing difficulties. Moreover, stresses relax by generating recombination active extended defects such as dislocations and grain boundaries that first of all reduce the efficiency and secondly induce very locally stress concentrations that reduce the mechanical stability of the solar cells. A new process based on a combination of laser crystallization of an amorphous silicon seed layer and epitaxial thickening of the seed layer by solid phase crystallization is being explored. Indeed, we measure by micro-Raman spectroscopy local stress concentrations including both compressive and tensile contributions inside grains and at grain boundaries in the laser crystallized seed layer. We attribute these stresses to particular defect configurations/structures since they do not correlate with both the misorientation inside grains and the low angle grain boundaries determined by electron backscatter diffraction. In most cases, the local stress concentrations in the seed layer are found to relax, presumably by structural rearrangements, during the solid phase epitaxy process. The structural evolution with respect to extended defect formation and stress built up during processing will be discussed.
Keywords: Stress, Raman, EBSD, Multicrystalline Silicon, Si-Films, Crystallization, Epitaxy, Defects.

1 INTRODUCTION

Thin films based photovoltaic (PV) technologies are considered to be able to achieve the goal of \$0.33/W_p (W_p = watt peak) required for the PV industry to impact the energy production landscape [1]. Manufacturing costs are reduced by combining low material consumption (no silicon wafers are necessary), single-panel and large-scale processing (1.38 m^2 glass substrates are used for instance by CSG Solar AG or even larger glass sheets of 5.7 m^2 are used e.g. at Sunfilm AG) [2, 3, 4], and advancements in materials and processes. A new approach to produce multicrystalline silicon (mc-Si) thin film solar cells on glass is being developed within the FP7 European project High-Ef [5, 6]. In this project, an amorphous silicon (a-Si) layer (100 – 500 nm thick) is melted and solidified by scanning a beam of a diode laser or eventually a diode laser array (final goal: 30 cm x 0.2 mm wide line focus) to form a multicrystalline seed layer with grains of several 100 μm^2. This seed layer is then epitaxially thickened (to >1 µm) by solid phase epitay (SPE). This combined laser crystallization (LC) and SPE process is expected to allow for solar cell efficiencies >10% due to comparably large, low defective grains and low stress levels in the silicon layer at competitive production costs. The latter goal can be achieved by using large glass substrates and electron beam evaporation at high rates. To achieve these goals, basic and applied breakthroughs are required.

A more focused stress engineering in thin film solar cells on foreign substrates is carried out by separating the intrinsic and extrinsic components of the stresses. The intrinsic stress is minimized by using optimal laser and solid phase crystallization parameters, since it depends on the preparation conditions and the resulting microstructure, while the extrinsic (thermal) stress is minimized by choosing a substrate with the thermal expansion coefficient close to that of crystalline silicon. Furthermore, the substrate should become soft during processing to allow stress relaxation and it should have a low thermal conductivity requiring low laser fluence during melting to avoid overheating which results in holes in the silicon seed layer [7]. The borosilicate glass (BSG) from Schott AG, namely Borofloat 33, has been found to meet these demands to a sufficiently good extent [8].

The present paper contributes to understanding the residual stresses and their relation to the microstructure in the thin film silicon, essentially the formation and arrangement of extended defects such as dislocations and all sorts of grain boundaries. For this purpose we combine micro-Raman spectroscopy (µRS) for measuring µm-scaled residual stress fields [9, 10] and electron backscatter diffraction (EBSD) in a scanning electron microscope (SEM) for evaluating the grain orientations and grain boundary types in mc-Si thin films on BSG substrates [11, 12]. Two types of samples have been investigated: laser crystallized silicon seed layers on glass (110 nm thick) and seed layers (705 nm thick) with a silicon layer from SPE that thickens the seed layer to a final thickness of 1.7 µm.

2 EXPERIMENTAL DETAILS

The seed layer samples were produced as follows: 80 nm amorphous SiN was deposited at CSG Solar AG [13] by plasma enhanced chemical vapor deposition (PECVD) on a 3 mm thick BSG substrate (Borofloat 33, Schott AG [8]). The next steps were performed at IPHT Jena. The SiN layer was thermally treated by scanning an excimer laser over the sample to remove the hydrogen from the layer. Thereafter, 110 nm to 700 nm thick a-Si layers were deposited by electron beam evaporation (EBE) of silicon. These layers are doped with boron by co-evaporation up to a doping level of 2.1×10^{19} cm^{-3}. The crystallization of the doped a-Si seed layers was carried out either with a diode laser from LIMO [14] with a 12 mm x 0.1 mm wide line focus, 806 nm wavelength, 14 kW/cm^2 laser power, and 6 cm/s scanning speed or with a diode laser from Rofin [15] with 0.8 mm x 0.3 mm wide line focus, 806 nm wavelength, 10 kW/cm^2 laser power,

and 5 cm/s scanning speed. The excimer laser tratement of the SiN layer prevents the hydrogen eruption during LC of the a-Si on top of it and thus the seed layer destruction during processing. The thinnest a-Si seed layer laser crystallized by the LIMO diode laser so far was 110 nm thick.

For epitaxial thickening we realized a preliminary seed plus SPE layer sample (for short: seed/epi sample) using this time 705 nm a-Si to form the seed layer followed by crystallization with the Rofin diode laser. 977 nm a-Si to serve after SPE as the epitaxial layer was deposited by EBE. The SPE process was carried out at 600 ^{o}C for 12h in a tube furnace.

The Raman stress measurements were performed as described in detail in Ref. 9. The focused laser spot had a diameter of ~ 1 µm and a penetration depth of a few µm in silicon for the used excitation wavelength of 633 nm so that the entire thickness of the samples is probed. The grain boundary pattern on the Raman stress maps is inferred from the Si peak intensity dependence on the crystallographic grain orientation [9]. The grains can be distinguished based on the fact that grains with different orientations show different overall Raman intensities. There are two approaches to evaluate the stress and its sign from the Raman Si peak shifts. In the case of large grained silicon, a stress-free position where the grain orientation can be accurately measured is readily available. Having the grain orientation, *several stress tensors components* can be determined using fixed polarization settings for incident and scattered light [9, 10]. This method will be applied in Sec. 3.1. However, *an average stress* can also be estimated independently of the grain orientation using unpolarized light and the following equation deduced for a crystalline silicon [100] wafer under biaxial stress [16]:

$$\sigma\ (\mathrm{MPa}) = -250\ \Delta\omega\ (\mathrm{cm}^{-1}) \qquad (1)$$

where $\sigma = (\sigma_{xx} + \sigma_{yy})/2$ with the in-plane stress components $\sigma_{xx} = \sigma_{yy}$ referring to the reference coordinate system shown in Figures 2 - 4 and $\Delta\omega = \omega_s - \omega_0$ with ω_0 being the peak position of the stress-free state and ω_s the peak position of the stressed state. This method will be applied in Sec. 3.1 and 3.2.

The grain orientations and grain boundary types were determined using an EBSD system from EDAX attached to a TESCAN LYRA XMU SEM. The inverse pole figure (unit triangle) displayed in Figure 1 (a) shows the sample normal direction relative to the axes of the measured crystal. As shown in Figure 1 (b), the grain boundaries (GBs) are classified into high angle GBs > 15^{o} and low angle GBs < 15^{o} using the misorientation angle between adjacent grains, that is, the rotation angle about the axis common to both lattices to bring them into coincidence, and in terms of Σ-values which denote the fraction of atoms in the GB plane coincident in both adjacent lattices [17].

3 RESULTS

3.1 Stress distribution in the seed layer sample

Typical stress distributions measured by µRS on the 110 nm thick seed layer are shown in Figures 2 and 3. They correspond to the regions of interest (ROI) marked on Figure 1 where the grain orientation, grain boundary type, and misorientations inside grains determined by EBSD are displayed. Since the seed layer is heavily boron-doped ($2.1\mathrm{x}10^{19}$ cm^{-3}) to serve as the solar cell emitter in a superstate cell concept, an additional Raman Si peak broadening due to the Fano effect occurs [18]. Thus, it is difficult to accurately determine Raman peak maxima positions and to translate the measured peak shifts into absolute stress values. Instead, lateral stress gradients are evaluated in form of stress-tensors or average values. The following difference stress tensors refering to the coordinate system shown in Figure 2 (a) have been obtained inside ROI 1:

$$\Delta\sigma_1 = \begin{pmatrix} -184\pm10 & -33\pm3 & 0 \\ -33\pm3 & -192\pm10 & 0 \\ 0 & 0 & -151\pm10 \end{pmatrix} MPa,$$

$$\Delta\sigma_2 = \begin{pmatrix} -200\pm10 & -51\pm3 & 0 \\ -51\pm3 & -213\pm10 & 0 \\ 0 & 0 & -152\pm10 \end{pmatrix} MPa.$$

These stress tensor measurements have been performed inside a large grain that shows an intergranular misorientation evolution as indicated by continuously changing color code in the respective EBSD mapping shown in Figure 1 (c). Such continuously changing crystal orientation behaviour can only be associated with dislocation networks that form low angle GBs indicated by arrows in ROI 1 [see Figure 1 (b)]. A second proof for the occurance of dislocation networks in such areas is the formation of poor pattern quality lines (not shown) in EBSD measurements. A third proof is the low crystallinity in these areas resulting in larger full width at half maximum (FWHM) values of the Si peak in µRS measurements as shown in Figure 2 (b). The intensity map of the Si peak taken by polarized µ-Raman (polarization direction of the incident laser light 15^{o} and the analyzer position setting the polarization direction of the scattered light on Y) is constant inside the investigated grain as shown in Figure 2 (c). Since the Raman intensity depends on the crystallographic orientation of the grain with respect to the polarization of the incident light, it is considered that in this case the intergranular misorientation measured by EBSD is too small to be detected by µ-Raman. The stress distribution inside this grain [Figure 2 (a)] does not correlate with both the misorientation [Figure 1 (c)] and the presence of low angle GBs [Figure 1 (b)] indicating that it is produced by a particular defect configuration/structure.

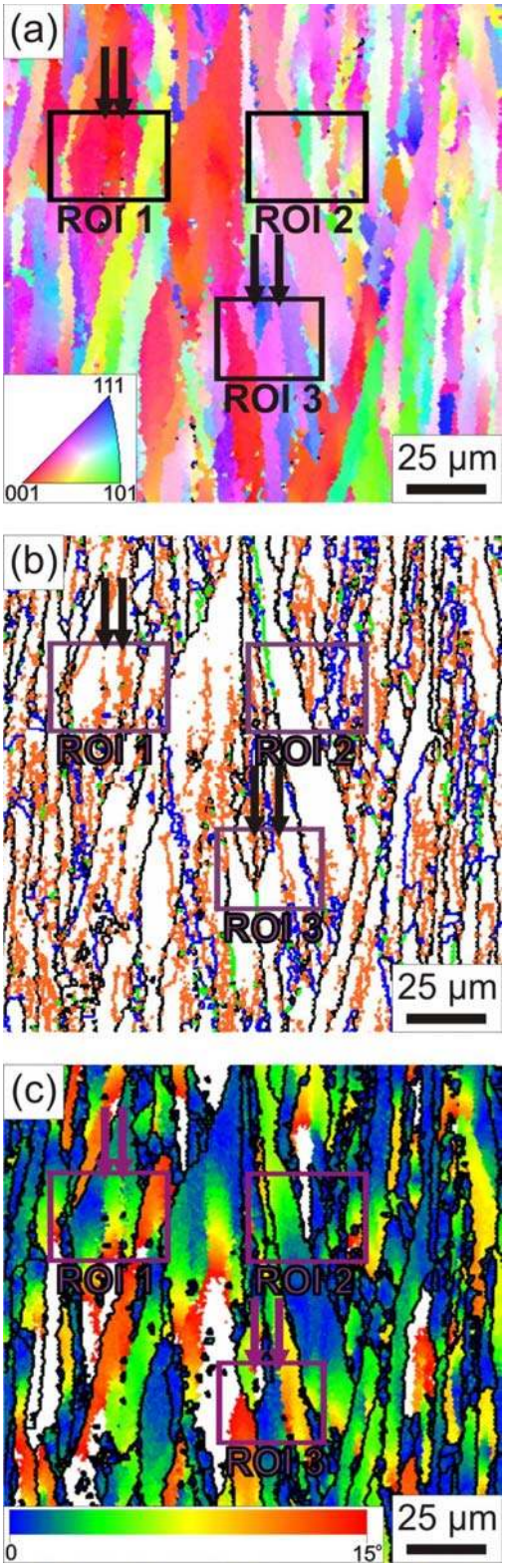

Figure 1: EBSD maps of the seed layer (110 nm thick, boron doping of 2.1×10^{19} cm^{-3}). The vertical arrows indicate identical features inside the regions of interest (ROI). (a) Inverse pole figure map. (b) Grain boundary map: (black lines) high angle GBs > 15°, (orange lines) low angle GBs < 15°, (blue lines) Σ3 GBs: 60° rotation around <111> axis, (green lines) Σ9 GBs: 38.9° rotation around <110> axis. (c) Intergranular misorientation gradient map.

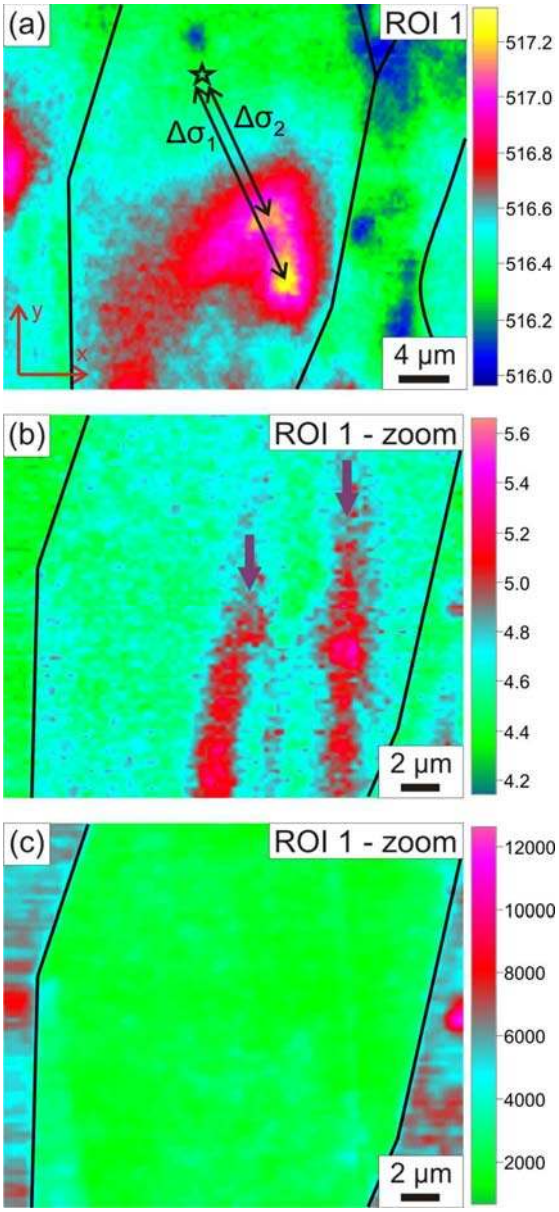

Figure 2: (a) Stress map of ROI 1 equivalent to Raman Si frequency shifts in cm^{-1}. The star marks the point where the grain orientation has been determined. Two lateral stress-tensor gradients ($\Delta\sigma_1$, $\Delta\sigma_2$) are indicated with respect to the reference coordinate system. (b, c) Maps of the full width at half maximum (FWHM) in cm^{-1} and intensity of the Raman Si peak in counts per second.

In the case of ROI 2 and 3, there is also no correlation between the stress maps (Figure 3) and the misorientation inside grains [Figure 1 (c)]. It is interesting to note here the existence of both stress and stress-free low angle GBs marked by arrows in Figures 1 and 3 (b). Inhomogeneous stress distributions including both compressive and tensile stresses have been found at GBs and inside grains being attributed to particular defect configurations/structures. Average lateral stress gradients up to 166 MPa shown in Figure 3 have been calculated using Eq. 1.

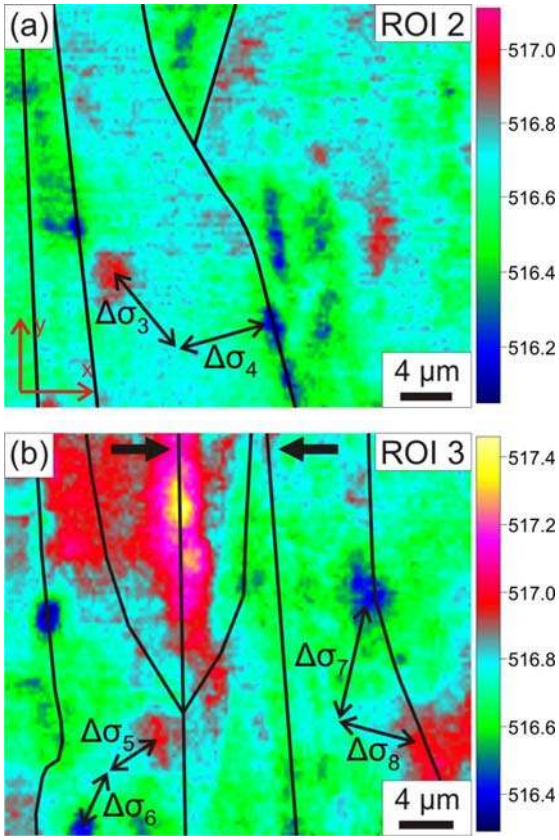

Figure 3: Stress maps of ROI 2 and 3 showing inhomogeneous stress distributions including both compressive (higher wavenumbers) and tensile (low wavenumbers) contributions at GBs and inside grains with respect to positions inside grains considered to be stress-free. The two horizontal arrows in (b) indicate stress and stress-free low angle GBs. Six lateral average stress gradients (± 12 MPa) with respect to the reference coordinate system obtained using Eq. 1 are shown: $\Delta\sigma_3$=58, $\Delta\sigma_4$=166, $\Delta\sigma_5$=48, $\Delta\sigma_6$=80, $\Delta\sigma_7$=83, and $\Delta\sigma_8$=55 MPa.

3.2 Stress distribution in the seed/epi sample

Typical stress distributions measured by µRS on the seed layer plus epilayer samples are shown in Figures 4 and 5. Similar to the seed sample, the seed layer is heavily boron-doped (6.27×10^{18} cm^{-3}) to serve as the solar cell emitter resulting in an additional doping-induced Raman Si peak broadening which makes accurate separation from the stress-induced peak shift more difficult [18]. The SPE leads to nonuniform stress distributions at GBs and inside grains without localized stress fields (see Figure 4) as compared to the sample with the seed layer only [see Figures 2 (a) and 3]. Average lateral stress gradients up to 212 MPa shown in Figure 4 have been evaluated using Eq. 1. Very localized stresses have been measured at GBs marked by dashed lines in Figure 5 where adjacent laser lines overlap during the laser crystallization of the seed layer. Micrometer wide elongated twins form in these regions as shown in the intensity map in Figure 5 (b).

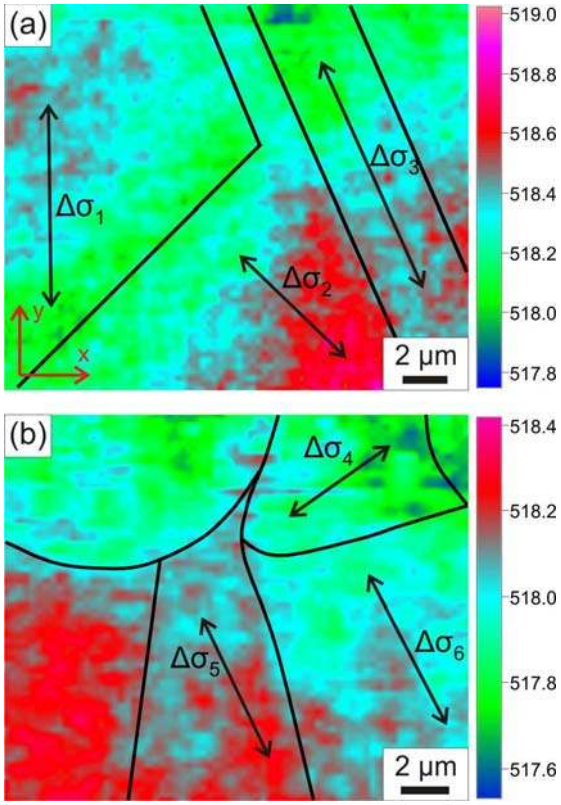

Figure 4: Stress maps of the seed/solid phase epitaxial sample showing inhomogeneous stress distributions at GBs and inside grains. Six lateral average stress gradients (± 12 MPa) with respect to the reference coordinate system obtained using Eq. 1 are displayed: $\Delta\sigma_1$=27, $\Delta\sigma_2$=141, $\Delta\sigma_3$=212, $\Delta\sigma_4$=97, $\Delta\sigma_5$=109, and $\Delta\sigma_6$=122 MPa.

4 DISCUSSIONS

4.1 Discussion on the origin and distribution of stresses in the seed layer sample

The seed layer is produced by laser melting and crystallization of a-Si on BSG substrates. Large grains in the several tens of micrometer diameter range can only be obtained when melting and re-crystallizing a-Si (requiring a temperature above 1412 °C) with sufficiently long time intervals where the silicon stays supercooled. These time intervals should be ms rather then ns. Moreover, low cooling rates and low nucleation rates at high growth rates of crystallites in the supercooled melt are required. These conditions can be obtained when using a continuous wave diode laser rather than formerly used pulsed excimer lasers [11, 12]. Low cooling rates can be obtained by dissipating heat into the glass substrate during laser irradiation that is transferred into the crystallizing silicon once the laser light resides already at other locations [7]. During heating and cooling of a-Si within the LC process, the BSG surface is heated and cooled with large gradients and thus the surface expands and shrinks as a result of the thermal expansion and contraction which produces thermal stresses inside the glass. The glass in the interior comes under tensile stress, while the glass surface stands under compressive stress. The exact temperatures of the BSG surface in

contact with melted silicon and the BSG interior are not known. They are considered to be close to the Si melting temperature and to the sample holder temperature of 690 ^{o}C, respectively. The stage heating turned out to be necessary to avoid high thermal stresses in the layer and substrate that lead to substantial crack formation. Since in this temperature range, both the glass surface and interior are soft/liquid [8] they can adapt their dimensions resulting in virtually no stress inside the glass. The possible remaining stress is further relaxed by keeping the glass above its annealing point of 560 ^{o}C for 15 min after the LC process. The cooling that follows must be carried out slowly so that no substantial temperature variations can occur between the surface and the interior that may leave behind any stress. Using this procedure no cracking of the BSG substrate and seed layer occurs.

The intrinsic stress build up in the seed layer due to amorphous-liquid-solid phase transitions in the course of the LC process are considered to be transffered to the soft BSG substrate. During cooling to room temperature, a uniformly distributed extrinsic tensile stress of ~ 3 MPa is predicted to be incorporated in the seed layer due to the difference in the thermal expansion coefficients between the crystalline silicon film and the BSG substrate [19]. Since local stress concentrations including both compressive and tensile stresses are measured at GBs and inside grains [see Figures 2 (a) and 3], they are considered to have mainly intrinsic origin being attributed to particular defect configurations/structures frozen-in during cooling to room temperature. These defects will be further investigated by transmission electron microscopy (TEM) to understand their formation mechanisms in order to avoid them by adjusting the LC parameters.

The presence of both stress and stress-free low angle GBs, marked by arrows in Figure 3 (b), which consist of dislocations can be explained by their local arrangement in configurations in which the superimposed long-range stress fields of the dislocations cancel partially or totally [20, 21].

4.2 Discussion on the origin and distribution of stresses in the seed/epi sample

The same procedure as described in Sec. 4.1 is used to obtain the seed layer for subsequent solid phase epitaxy while keeping the BSG substrate and the seed layer crack free. If the defect structures leading to local stress concentrations at GBs and inside grains [see Figures 2 (a) and 3] would be still present in the seed layer after epitaxial thickening, they should be detected by µRS. Since this is not the case, it is considered that these intrinsic stresses relax by structural rearrangements during the SPE process [22] resulting in extended stress distributions as shown in Figure 4. This represents an important step towards low stress mc-Si thin films for solar cells. However, stress measurements on both the seed layer and the seed/epi layers system at identical positions are needed to clarify this point. The extrinsic stress build up in the seed layer during cooling from LC temperature to room temperature is transferred to the soft BSG during the SPE process. Intrinsic tensile stress is incorporated in the epi-layer with respect to the seed layer due to the amorphous-solid phase transformation in the course of SPE. This stress can not be transferred to the solid underlying seed layer or even the BSG substrate. An additional extrinsic tensile stress of ~ 3 MPa is predicted to be integrated in the seed/epi layers system during cooling from the SPE temperature of 600 ^{o}C to room temperature due to the difference in the thermal expansion coefficients between the crystalline silicon film and the BSG substrate [19]. Indeed, the presence of an overall tensile stress is confirmed by the shift of the Raman silicon peak to lower wavenumbers with respect to that of a single crystalline silicon wafer at ~ 520.9 cm^{-1} which is often used as a stress-free reference. However, the boron doping-induced peak broadening tends to move peak maxima also to lower wavenumbers and this inaccuracy can not easily be avoided. In spite of the apparent structural relaxation during SPE, the lateral average stress gradients are on average slightly larger for the seed/epi sample (118 MPa, Figure 4) than for the seed sample (90 MPa, Figure 3).

It is also interesting to point out that mechanically weak regions develop in adjacent laser scan lines where irradiated areas overlap. Here, micrometer wide elongated twins form with very localized stresses around their boundaries as shown in Figure 5 (a). Therefore, the development of a new laser diode array tool with a line focus of 30 cm within the FP7 High-Ef project will not only increase the yield but it will also decrease the number of overlapping areas resulting in an improved mechanical stability.

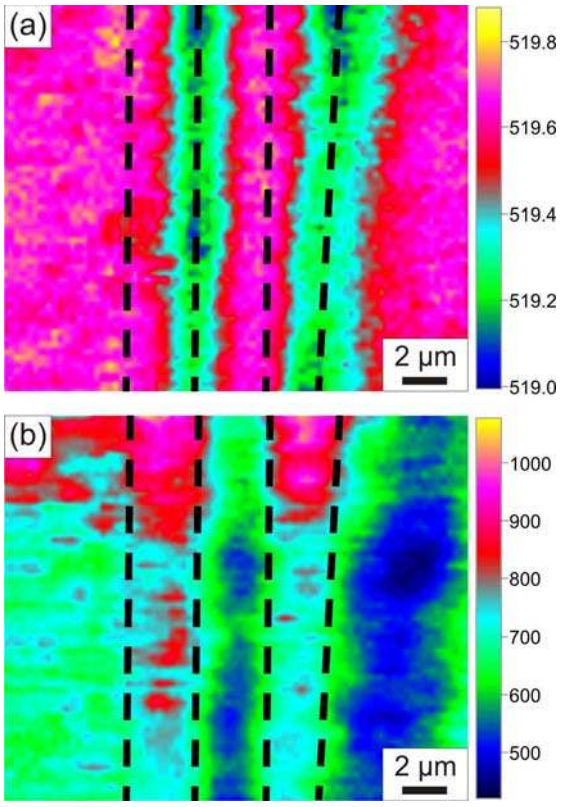

Figure 5: (a) Stress map of the seed/solid phase epitaxial sample showing very localized stresses at twin boundaries indicated by dashed lines in laser overlapping areas of adjacent scan lines formed during the LC of the seed layer. (b) Intensity map of the Raman Si peak where micrometer wide elongated twins are visible. The change in intensity along the twin grains is attributed to an intergranular misorientation.

5 CONCLUSIONS

Micro-Raman spectroscopy has proven to be an effective method to quantify the residual stresses and to visualize their distribution in mc-Si thin films on glass based on the frequency shifts of the Raman Si peak. The laser crystallization process leads to local stress concentrations up to 166 MPa at GBs and inside grains including both compressive and tensile contributions. These stresses do not correlate with both the misorientation inside grains and the low angle GBs determined by EBSD suggesting that they are produced by particular defect configurations/structures. Low angle GBs represent another source of internal stresses when the dislocations forming them arrange in configurations in which their superimposed long-range stress fields do not cancel totally or at all. Localized stresses develop also at twin boundaries formed in laser overlapping areas of adjacent scan lines during the laser crystallization of the seed layer. Stress measurements on a preliminary seed/solid phase epitaxial sample suggest that the local stress concentrations in the seed layer relax in the course of solid phase epitaxy except for those stresses at twin boundaries in laser overlapping areas.

6 ACKNOWLEDGMENTS

This work was financially supported by the European Commission within the FP7-Energy project High-Ef and by the Max-Planck Society within the project Nanostress. The authors would like to thank F. Falk for fruitful discussions.

6 REFERENCES

[1] D. Ginley, M. A. Green, and R. Collins, MRS Bull. 33 (2008) 355.
[2] M.A. Green, P.A. Basore, N. Chang, D. Clugston, R. Egan, R. Evans, D. Hogg, S. Jarnason, M. Keevers, P. Lasswell, J. O'Sullivan, U. Schubert, A. Turner, S.R. Wenham, and T. Young, Solar Energy 77 (2004) 857.
[3] P.A. Basore, In Proceedings of the 21st European Photovoltaic Solar Energy Conference, Dresden (2006) p. 544.
[4] http://www.sunfilm.com/en/products/.
[5] F. Falk et al., this conference 3CO.6.2.
[6] www.high-ef.eu.
[7] G. Andrä and F. Falk, phys. stat. sol. (c) 5 (2008) 3221.
[8]www.schott.com/hometech/english/download/brochure_borofloat_e.pdf, accessed 19 August 2009.
[9] G. Sarau, M. Becker, G. Andrä, and S. Christiansen, In Proceedings of the 23rd EU PVSEC, Valencia, Spain (2008) p. 2265.
[10] M. Becker, H. Scheel, S. Christiansen, and H. P. Strunk, J. Appl. Phys. 101 (2007) 063531.
[11] M. Nerding, S. Christiansen, R. Dassow, K. Taretto, J.R. Köhler, and H. P. Strunk, Solid State Phenomena 93 (2003) 173.
[12] S. Christiansen, P. Lengsfeld, J. Krinke and M. Nerding, J. Appl. Phys. 89 (2001) 5348.
[13] www.csgsolar.com.
[14] www.limo.de.
[15] www.rofin.com.
[16] I. De Wolf, Semicond. Sci. Technol. 11 (1996) 139.
[17] H. Grimmer, W. Bollmann, and D. H. Warrington, Acta Crystallog. A30 (1974) 197.
[18] N. H. Nickel, Laser Crystallization of Silicon, Elsevier (2003) Chapter 5.
[19] G. Sarau et al., manuscript in preparation.
[20] D. Hull and D. J. Bacon, Introduction to Dislocations, Butterworth-Heinemann (2001), Chapter 4 and 9.
[21] G. Sarau et al., this conference 2AO.3.3.
[22] Y. Masaki, P. G. LeComber, and A. G. Fitzgerald, J. Appl. Phys. 74 (1993) 129.